Energy spectrum and quantum Hall effect in twisted bilayer graphene

Pilkyung Moon and Mikito Koshino
Department of Physics, Tohoku University, Sendai, 980–8578, Japan
(Received 20 February 2012; published 29 May 2012)

We investigate the electronic structure and the quantum Hall effect in twisted bilayer graphenes with various rotation angles in the presence of magnetic field. Using a low-energy approximation, which incorporates the rigorous interlayer interaction, we computed the energy spectrum and the quantized Hall conductivity in a wide range of magnetic field from the semiclassical regime to the fractal spectrum regime. In weak magnetic fields, the low-energy conduction band is quantized into electronlike and holelike Landau levels at energies below and above the van Hove singularity, respectively, and the Hall conductivity sharply drops from positive to negative when the Fermi energy goes through the transition point. In increasing magnetic field, the spectrum gradually evolves into a fractal band structure called Hofstadter's butterfly, where the Hall conductivity exhibits a nonmonotonic behavior as a function of Fermi energy. The typical electron density and magnetic field amplitude characterizing the spectrum monotonically decrease as the rotation angle is reduced, indicating that the rich electronic structure may be observed in a moderate condition.

DOI: 10.1103/PhysRevB.85.195458 PACS number(s): 72.80.Vp, 73.20.−r, 73.43.−f

I. INTRODUCTION

The electronic structure of bilayer graphene is highly sensitive to the stacking geometry between the two layers. The interlayer interaction in bilayer graphene with regular AB stacking[1–3] modifies the linear dispersion of monolayer graphene into the quadratic dispersion, where an electron behaves as a massive particle.[4] On the other hand, the recent epitaxial growth technique[5,6] realized twisted bilayer graphene (TBG) in which two layers are stacked with a random rotation angle.[6–8] The unit-cell area of TBG can be more than 1000 times as large as that of monolayer graphene, due to slightly misoriented lattice vectors of two layers. Such an atomic configuration was observed as Moiré pattern in the scanning tunneling microscopy.[9–13] TBG was also fabricated in different methods such as folding of mechanically exfoliated graphenes,[14] segregation of graphene on Ni film,[9] and unzipping of carbon nanotube.[15]

The electronic structure of TBG shows a linear band dispersion near Dirac points[7,16–19] rather than the massive dispersion of AB-stacked bilayer, suggesting relatively weak interlayer interaction. In strong magnetic fields, however, it is predicted that the spectrum exhibits a fractal structure called Hofstadter's butterfly, in which a series of energy gaps appear in a self-similar fashion.[20,21] The fractal band structure generally occurs in a periodic system when the magnetic flux per a unit cell is comparable to h/e, and this condition is realized in TBG in a reasonable magnetic field range owing to the large unit cell. The fractal band structure and the quantum Hall effect were theoretically studied for TBG in the strong magnetic field regime using a continuous interlayer coupling model.[21] Experimentally, the energy spectrum of the twisted graphene stacks in magnetic field was probed in the transport measurement[22,23] and the magneto-optical absorption,[24] while the fractal band structure has not yet been observed.

In this paper, we investigate the electronic spectrum and the quantum Hall effect in TBG with various rotation angles and magnetic fields. We calculate the spectrum by including a limited number of bases which are significant in the low-energy spectrum, while rigorously taking account of transfer integrals between lattice points on the different layers. Using this method, we describe the spectral evolution in a wide range of magnetic field, from the semiclassical Landau levels in the weak-field regime to the fractal band structure in the strong-field regime.

In weak magnetic fields, we find that the low-energy conduction band is quantized into electronlike and holelike Landau levels at energies below and above the van Hove singularity, respectively, in accordance with the topological change of the Fermi surface from electron type to hole type at the band saddle point. As a consequence, the quantized Hall conductivity abruptly jumps from positive to negative when the Fermi energy goes through the transition point. In increasing magnetic field, the electron and hole Landau levels begin to be mixed and gradually evolve into the fractal band structure. We calculate the quantized Hall conductivity for each single gap, and demonstrate that it changes nonmonotonically as a function of Fermi energy and magnetic field.[25,26]

II. THEORETICAL METHODS

A. Atomic structure

TBG is characterized by the relative rotation angle θ and the relative translation vector between two graphene layers. When the lattice structures of the two layers are commensurate, we can define the primitive lattice vectors $\mathbf{L}_1$ and $\mathbf{L}_2$ as the least common multiples of the unit vectors on the two layers. $\mathbf{L}_1$ is written by integers m,n,m',n' as[27]

$$\mathbf{L}_1 = m\mathbf{a}_1^{(1)} + n\mathbf{a}_2^{(1)} = m'\mathbf{a}_1^{(2)} + n'\mathbf{a}_2^{(2)}, \tag{1}$$

where $\mathbf{a}_1^{(l)}$ and $\mathbf{a}_2^{(l)}$ are the lattice vectors of the layer $l = 1,2$ defined in Fig. 1(a). $\mathbf{L}_2$ is obtained by rotating $\mathbf{L}_1$ by 60°. By appropriate choice of lattice vectors $\mathbf{a}_i^{(l)}$, the indices (m',n') can be made equal to (n,m), and thus TBG is specified by a single pair of integers (m,n). The rotation angle θ is related to (m,n) by

$$\cos\theta = \frac{1}{2}\frac{m^2+n^2+4mn}{m^2+n^2+mn}, \tag{2}$$

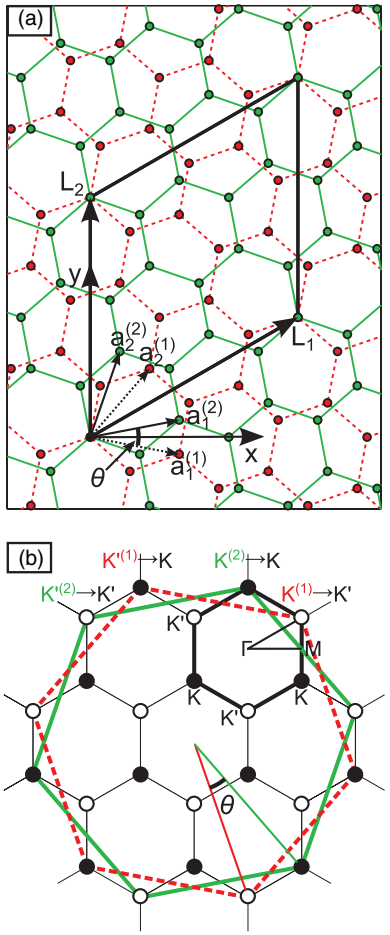

FIG. 1. (Color online) (a) Atomic structure of TBG with rotation angle $\theta = 21.8^\circ$. Dashed (red) and solid (green) lines represent the lattices of layers 1 and 2, respectively. (b) Brillouin zone of TBG with $\theta = 21.8^\circ$. Dashed (red) and solid (green) large hexagons correspond to the first Brillouin zone of layers 1 and 2, respectively, and thick small hexagon to the reduced Brillouin zone of TBG. Open and filled circles are two inequivalent valleys K and K' of TBG.

and the lattice constant $L = |\mathbf{L}_1| = |\mathbf{L}_2|$ by

$$L = a\sqrt{m^2 + n^2 + mn} = \frac{|m-n|}{2\sin(\theta/2)}a, \tag{3}$$

where $a = |\mathbf{a}_1| = |\mathbf{a}_2| \approx 0.246$ nm is the lattice constant of monolayer graphene. The area of TBG unit cell is given by $S = |\mathbf{L}_1 \times \mathbf{L}_2| = (\sqrt{3}/2)L^2$.

Figure 1(a) shows the atomic structure of TBG with $(m,n) = (1,2)$ and $\theta = 21.8^\circ$. Throughout the paper, we set the coordinates (x,y) on the graphene plane so that the y axis is parallel to $\mathbf{L}_2$, and z to the direction perpendicular to the plane. We ignore the relative translation between two layers, which makes a minor difference in the electronic structure when the unit cell is large enough.

Figure 1(b) shows the extended Brillouin zone of TBG with $\theta = 21.8^\circ$. The two large hexagons represent the first Brillouin zones of layers 1 and 2, respectively. $K^{(l)}$ and $K'^{(l)}$ denote the two inequivalent corners of layer l, which are Dirac points in the single-layer band structure. The four Dirac points of $K^{(1)}$, $K'^{(1)}$, $K^{(2)}$, and $K'^{(2)}$ are folded back to two Dirac points, K and K', in the reduced Brillouin zone.[28]

Figure 2 shows the atomic structures of four different TBGs to be considered in following sections. They are specified by $(m,n) = (3,4),(8,9),(12,13)$, and $(22,23)$, and the rotation angles $\theta = 9.43^\circ$, 3.89°, 2.65°, and 1.47°, respectively. As the angle θ decreases, the size of the unit cell enlarges and the Moiré pattern becomes evident.

B. Tight-binding model

In a tight-binding model in terms of p_z atomic orbitals, the Hamiltonian of TBG at zero magnetic field is written as

$$H_{\mathrm{TBG}}^{B=0} = -\sum_{\langle i,j\rangle} t(\mathbf{R}_i,\mathbf{R}_j)|\Psi_i\rangle\langle\Psi_j| + \mathrm{H.c.}, \tag{4}$$

where $\mathbf{R}_i$ and $|\Psi_i\rangle$ represent the lattice point and the atomic state at site i, respectively, and $t(\mathbf{R}_i,\mathbf{R}_j)$ is the transfer integral

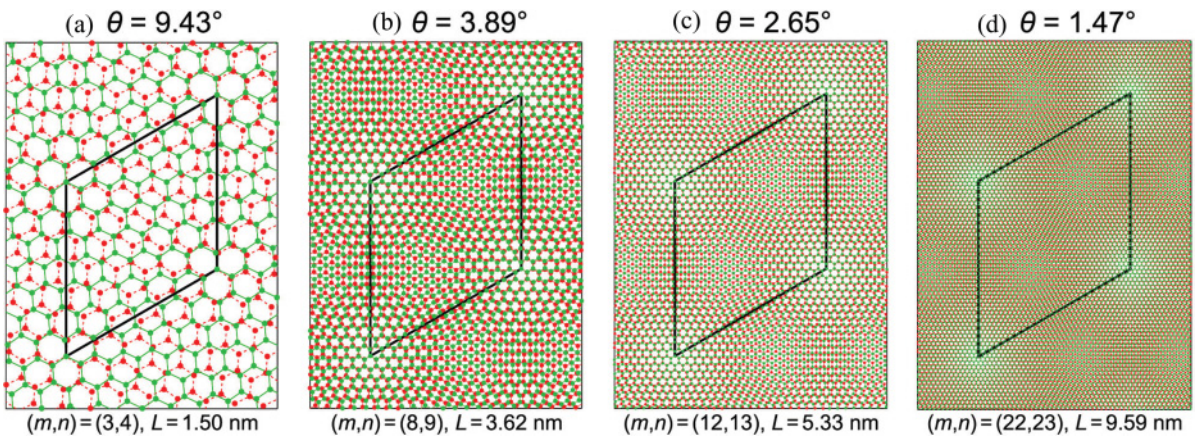

FIG. 2. (Color online) Atomic structure of TBG with rotation angles of (a) 9.43°, (b) 3.89°, (c) 2.65°, and (d) 1.47°. Dashed (red) and solid (green) lines represent lattices of layers 1 and 2, respectively. (m,n) is the index characterizing the primitive lattice vector of TBG, and L is the length of the lattice vector.

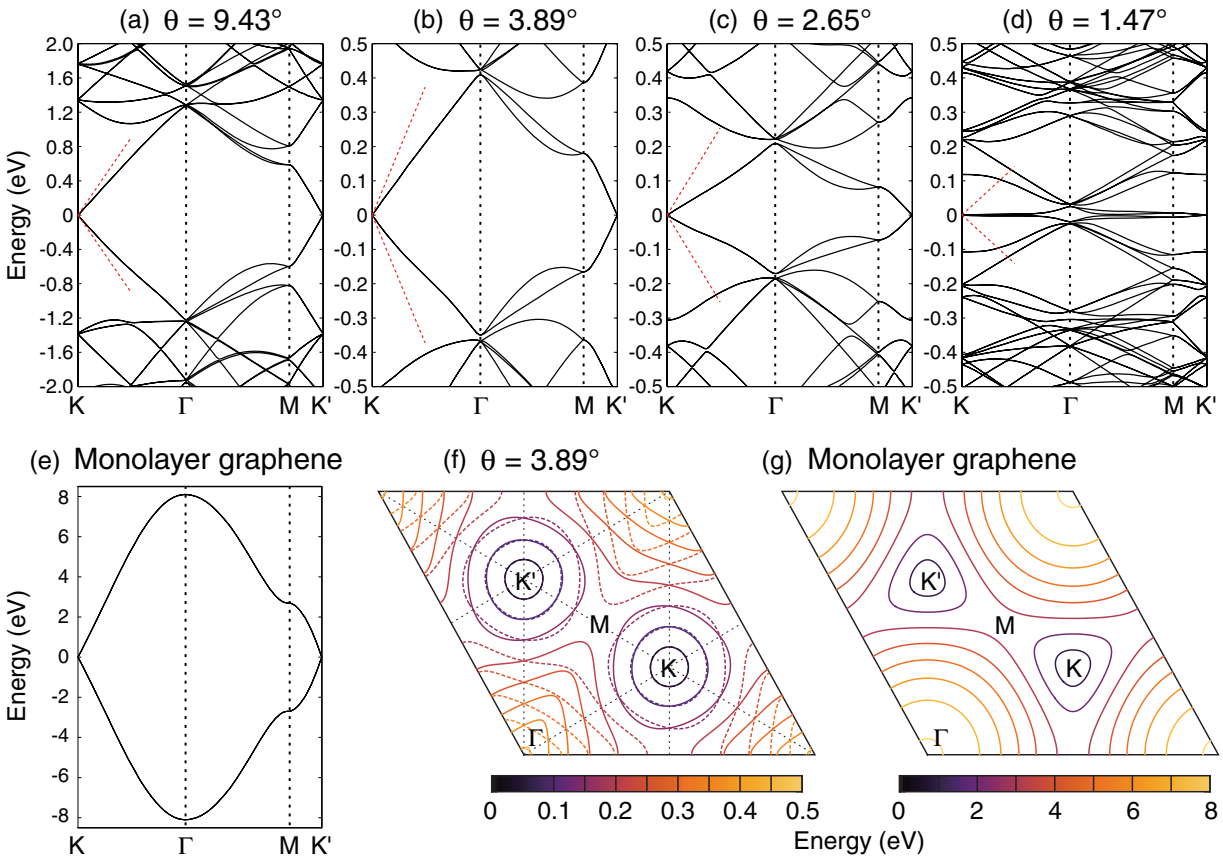

FIG. 3. (Color online) Band structure of TBG with rotation angles (a) 9.43°, (b) 3.89°, (c) 2.65°, (d) 1.47°, and that of (e) monolayer graphene. Dashed (red) slopes around the K point indicate the monolayer's band dispersion. Note that the scale of wave number (horizontal axis) reduces as the the rotation angle decreases. Dirac point energy is set to zero. (f) Contour plot of the two lowest conduction bands of TBG with $\theta = 3.89°$. (g) Corresponding plot for the conduction band of monolayer graphene.

between the sites i and j. We adopt an approximation[29–32]

$$-t(\mathbf{R}_i,\mathbf{R}_j) = V_{pp\pi}\left[1-\left(\frac{\mathbf{d}\cdot\mathbf{e}_z}{d}\right)^2\right] + V_{pp\sigma}\left(\frac{\mathbf{d}\cdot\mathbf{e}_z}{d}\right)^2,$$
$$V_{pp\pi} = V^0_{pp\pi}\exp\left(-\frac{d-a_0}{\delta}\right), \quad (5)$$
$$V_{pp\sigma} = V^0_{pp\sigma}\exp\left(-\frac{d-d_0}{\delta}\right),$$

where $\mathbf{d} = \mathbf{R}_i - \mathbf{R}_j$, and $\mathbf{e}_z$ is the unit vector parallel to the z axis. $V^0_{pp\pi}$ is the transfer integral between the nearest-neighbor atoms of monolayer graphene which are located at distance $a_0 = a/\sqrt{3} \approx 0.142$ nm, and $V^0_{pp\sigma}$ is the interlayer transfer integral between vertically located atoms at the interlayer distance $d_0 \approx 0.335$ nm. Here, we take $V^0_{pp\pi} \approx -2.7$ eV, $V^0_{pp\sigma} \approx 0.48$ eV, to fit the low-energy dispersion of bulk graphite. δ is the decay length of the transfer integral, and is chosen as $0.184a$ so that the next-nearest intralayer coupling becomes $0.1V^0_{pp\pi}$.[30,32] The transfer integral for $d > 4a_0$ is exponentially small and can be safely neglected. The band velocity of the Dirac cone in monolayer graphene is given by

$$v \approx \frac{\sqrt{3}}{2}\frac{V^0_{pp\pi}}{\hbar}. \quad (6)$$

We plot the energy bands of four TBGs with the different rotation angles in Figs. 3(a)–3(d). Dashed (red) lines near the K point indicate the band dispersion of monolayer graphene, of which the entire structure is shown in Fig. 3(e). The low-energy spectrum can be understood by folding monolayer's Dirac cone into the reduced Brillouin zone, and thus the structures are similar among different rotation angles except for the scale. The lowest band is characterized by a linear dispersion analogous to monolayer's band,[7,16–19] the van Hove singularity at the M point,[10,19,33,34] and a holelike pocket at the Γ point. In accordance with the band-folding picture, the width of the lowest band is roughly given by $4\pi\hbar v/(3L)$, which is the graphene's band gradient times the distance between K and Γ. In small rotation angles less than 5°, however, the width becomes significantly smaller than this estimate because the level repulsion from the upper bands becomes comparable to the bandwidth itself. As a result, the velocity of the Dirac cone gradually reduces from the monolayer's v. In the smallest rotation angle $\theta = 1.47°$, in particular, the lowest energy band is highly distorted, and nearly flat dispersion appears near zero energy.[32,35]

The lowest band of TBG is composed of a pair of nearly degenerate branches. Figure 3(f) shows the contour plots of the two lowest conduction bands in $\theta = 3.89°$. Those two bands, indicated by solid and broken curves, are mirror symmetric to

each other with respect to the lines of $K-\Gamma$, $K'-\Gamma$, and $K-K'$, reflecting the C_2 symmetry in the real-space lattice structure. Each of the two bands has a similar landscape to that of monolayer graphene, which is shown in Fig. 3(g), where the linear dispersion, the saddle point, and the hole pocket appear near $K(K')$, M, and Γ, respectively.

C. Electronic structures in magnetic fields

We consider TBG in a uniform magnetic field $\mathbf{B}=(0,0,B)$ perpendicular to the layer. For simplicity, we neglect spin Zeeman splitting throughout the paper. The system is characterized by the number of magnetic flux per a unit cell, $\Phi=BS$, measured in units of the flux quantum $\Phi_0=h/e$. In the magnetic field, the Hamiltonian is no longer translationally symmetric because of the spatial dependence of the vector potential. When Φ/Φ_0 is a rational number p/q (p and q are co-prime integers), however, we can introduce a magnetic unit cell with lattice vectors $\tilde{\mathbf{L}}_1=q\mathbf{L}_1$ and $\tilde{\mathbf{L}}_2=\mathbf{L}_2$, and construct the eigenstates so as to satisfy the magnetic Bloch condition.[36,37] By choosing the vector potential as $\mathbf{A}=(0,Bx,0)$ and taking the y axis parallel to $\mathbf{L}_2$, the magnetic Bloch condition for TBG is written as

$$\begin{aligned}\Psi_{\mathbf{k}}(\mathbf{r}+\tilde{\mathbf{L}}_1)&=e^{i\mathbf{k}\cdot\tilde{\mathbf{L}}_1}e^{-i(e/\hbar)(\mathbf{A}-\mathbf{B}\times\mathbf{r})\cdot\tilde{\mathbf{L}}_1}\Psi_{\mathbf{k}}(\mathbf{r}),\\ \Psi_{\mathbf{k}}(\mathbf{r}+\tilde{\mathbf{L}}_2)&=e^{i\mathbf{k}\cdot\tilde{\mathbf{L}}_2}\Psi_{\mathbf{k}}(\mathbf{r}),\end{aligned}\tag{7}$$

where $\mathbf{k}$ is the Bloch wave number defined in the magnetic Brillouin zone spanned by reciprocal vectors of $\tilde{\mathbf{L}}_1$ and $\tilde{\mathbf{L}}_2$. Since the magnetic unit cell is q times as large as the unit cell in the absence of magnetic field, the magnetic Brillouin zone is q-fold of the original, and each energy band at zero magnetic field splits into q subbands.[20]

The tight-binding Hamiltonian under a magnetic field is obtained by adding a phase factor to the transfer integral in Eq. (4). This is written as

$$\begin{aligned}H_{\mathrm{TBG}}&=-\sum_{\langle i,j\rangle}t(\mathbf{R}_i,\mathbf{R}_j)e^{i\phi_{ij}}|\Psi_i\rangle\langle\Psi_j|+\mathrm{H.c.},\\ \phi_{ij}&=-\frac{e}{\hbar}\int_{\mathbf{R_j}}^{\mathbf{R_i}}\mathbf{A}(\mathbf{r})\cdot d\mathbf{r}.\end{aligned}\tag{8}$$

It is, however, not practical to calculate the energy spectrum of TBG by diagonalizing this Hamiltonian since the number of atoms in a magnetic unit cell is huge in feasible magnetic fields. Instead, we construct the basis from the effective-mass wave functions for Landau levels of monolayer graphene, which approximate the eigenstates in the absence of the interlayer coupling. We then truncate the bases far from the Dirac point, and compose the Hamiltonian matrix by writing H_{TBG} in terms of the reduced basis.

In monolayer graphene under magnetic field, the eigenstates are labeled by (v,n,k_y) with the valley index $v=K,K'$, the Landau level index $n=0,\pm1,\ldots$, and the wave vector k_y along the y direction.[38–42] The eigenenergy depends only on n as

$$\varepsilon_n=\hbar\omega_B\ \mathrm{sgn}(n)\sqrt{|n|},\tag{9}$$

with $\hbar\omega_B=\sqrt{2\hbar v^2eB}$. The effective wave functions are written as[39,40]

$$\begin{aligned}\mathbf{F}_{Knk_y}(\mathbf{r})&=\frac{C_n}{\sqrt{L}}e^{ik_yy}\begin{pmatrix}\mathrm{sgn}(n)(-i)\phi_{|n|-1,k_y}(x)\\ \phi_{|n|,k_y}(x)\\ 0\\ 0\end{pmatrix},\\ \mathbf{F}_{K'nk_y}(\mathbf{r})&=\frac{C_n}{\sqrt{L}}e^{ik_yy}\begin{pmatrix}0\\ 0\\ \phi_{|n|,k_y}(x)\\ \mathrm{sgn}(n)(-i)\phi_{|n|-1,k_y}(x)\end{pmatrix}.\end{aligned}\tag{10}$$

Here, $\mathbf{F}=(F_A^K,F_B^K,F_A^{K'},F_B^{K'})$ is a four-component vector representing the envelope function of each site and valley. We defined $\phi_{n,k}(x)=(2^n n!\sqrt{\pi}l_B)^{-1/2}\ e^{-z^2/2}H_n(z)$, with $z=(x+kl_B^2)/l_B$ and H_n being the Hermite polynomial, $l_B=\sqrt{\hbar/(eB)}$, and

$$\begin{aligned}C_n&=\begin{cases}1 & (n=0),\\ 1/\sqrt{2} & (n\neq0),\end{cases}\\ \mathrm{sgn}(n)&=\begin{cases}0 & (n=0),\\ n/|n| & (n\neq0).\end{cases}\end{aligned}\tag{11}$$

The tight-binding wave function Ψ on the layer l can be expressed in terms of the envelope function $\mathbf{F}$ as[42]

$$\begin{aligned}\Psi_A(\mathbf{R}_A)&=e^{i\mathbf{K}^{(l)}\cdot\mathbf{R}_A}F_A^K(\mathbf{R}_A)+e^{i\eta^{(l)}}e^{i\mathbf{K}'^{(l)}\cdot\mathbf{R}_A}F_A^{K'}(\mathbf{R}_A),\\ \Psi_B(\mathbf{R}_B)&=-\omega e^{i\eta^{(l)}}e^{i\mathbf{K}^{(l)}\cdot\mathbf{R}_B}F_B^K(\mathbf{R}_B)+e^{i\mathbf{K}'^{(l)}\cdot\mathbf{R}_B}F_B^{K'}(\mathbf{R}_B),\end{aligned}\tag{12}$$

where $\eta^{(l)}$ is the angle of $\mathbf{a}_1^{(l)}$ to the x axis. We define $\Psi^{(l)}_{vnk_y}$ as the tight-binding wave function on the layer l generated from $\mathbf{F}_{vnk_y}$.

We then combine the bases of different k_y so as to satisfy the magnetic Bloch condition, Eq. (7). We define

$$\begin{aligned}\Psi^{(l)}_{vn\mathbf{k}m}&=\sum_{j=-\infty}^{\infty}\alpha^j\exp\left[i\pi pq\frac{j(j+1)}{2}\right]\Psi^{(l)}_{vnk_y^{(m)}},\\ \alpha&=\exp\left[i\left(\mathbf{k}-\mathbf{K}_v^{(l)}\right)\cdot\left(\tilde{\mathbf{L}}_1-\frac{q}{2}\tilde{\mathbf{L}}_2\right)\right],\\ k_y^{(m)}&=k_y-\left(\mathbf{K}_v^{(l)}\right)_y-\frac{2\pi}{L_y}(pj+m),\end{aligned}\tag{13}$$

where $\mathbf{k}$ is the Bloch wave number defined in the magnetic Brillouin zone, $m=0,1,\ldots,p-1$, and $\mathbf{K}_v^{(l)}$ represent $\mathbf{K}^{(l)},\mathbf{K}'^{(l)}$ for $v=K,K'$, respectively. It is straightforward to show that this satisfies the condition of Eq. (7).

An eigenstate of TBG is written as a linear combination of single-layer eigenstates $\Psi^{(l)}_{vn\mathbf{k}m}$ belonging to the same $\mathbf{k}$. We only include single-layer bases within $-E_{\max}<\varepsilon_n<E_{\max}$ to discard the bases which do not much affect the low-energy spectrum. The eigenenergies are obtained by diagonalizing the Hamiltonian matrix within the reduced bases

$$H_{\mathbf{k}}[(l,v,n,m),(l',v',n',m')]\equiv\left\langle\Psi^{(l)}_{vn\mathbf{k}m}\middle|H_{\mathrm{TBG}}\middle|\Psi^{(l')}_{v'n'\mathbf{k}m'}\right\rangle\tag{14}$$

for each $\mathbf{k}$ in the magnetic Brillouin zone. The cutoff energy should be sufficiently larger than the interlayer-coupling

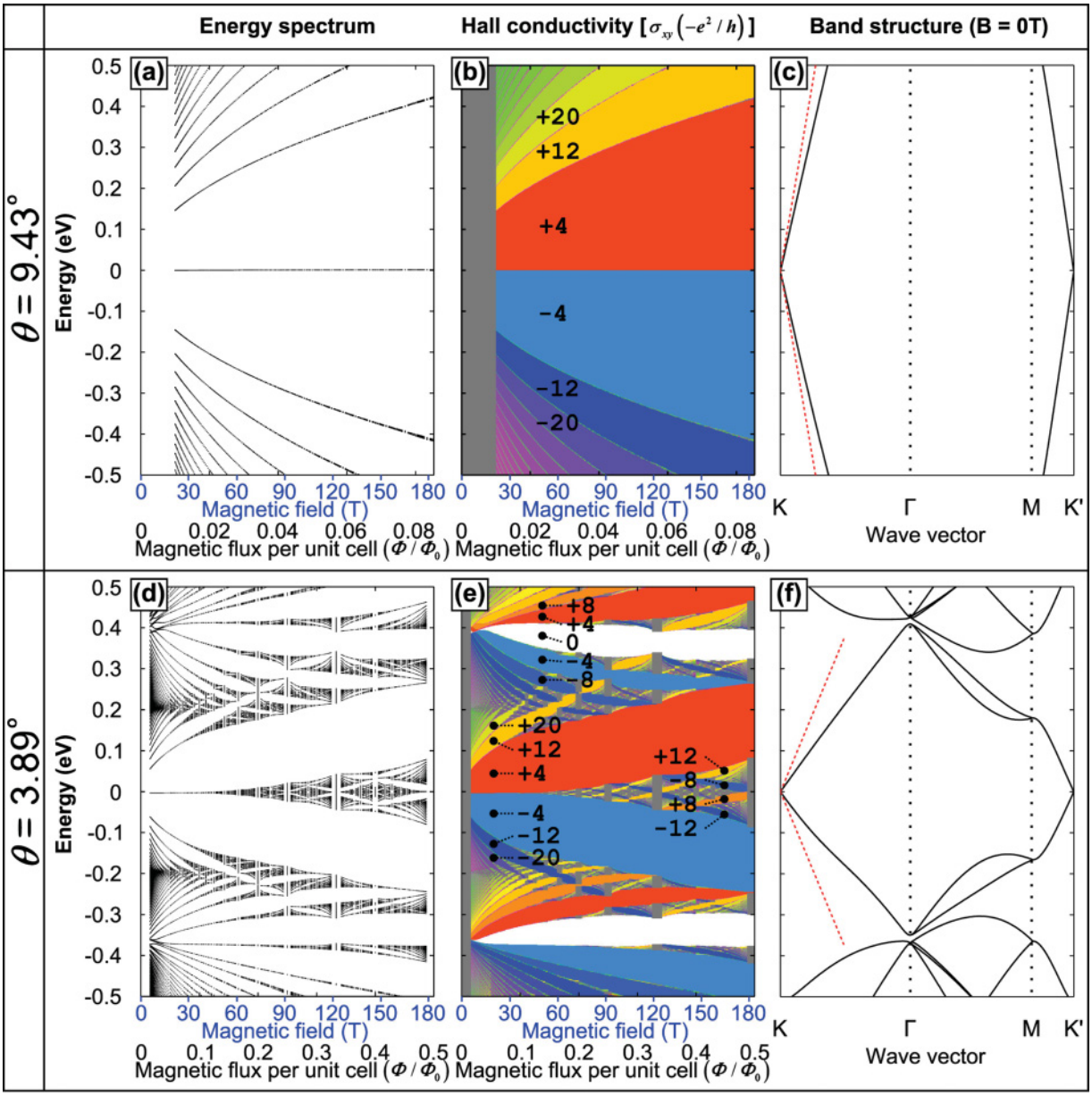

FIG. 4. (Color online) Energy spectrum and quantum Hall effect in TBG in magnetic field with rotation angles of 9.43° (above) and 3.89° (below). In each row, the left and middle panels display the energy spectrum and the quantized Hall conductivity as functions of magnetic field strength, respectively, and the right panel shows the band structure in the absence of magnetic field. Dashed (red) slopes around the K point indicate the dispersion of monolayer graphene. In (b) and (e), the quantized values of Hall conductivity inside energy gaps are indicated by numbers as well as colors filling the gaps. The Hall conductivity of the gray area can not be determined by the present calculation.

energy, which is of the order of $V^0_{pp\sigma}$ at most, and tends to decrease in small twisting angles. Here, we take $E_{\max} = 1.5$ eV for $\theta = 9.43°$ and 3.89°, and 1.0 eV for 2.65° and 1.47°. To avoid undesired effects caused by a discrete change in the number of bases in varying magnetic field, we adopt a soft cutoff which gradually reduces the matrix elements associated to the single-layer bases beyond $\pm E_{\max}$.

We calculate the matrix elements [Eq. (14)] between different layers by evaluating the transfer integral for each pair of carbon atoms up to the cutoff distance $d = 4a_0$. The matrix elements within the same layer can be replaced with a diagonal matrix composed of the effective-mass eigenenergies in monolayer graphene,

$$H_{\mathbf{k}}[(l,v,n,m),(l,v',n',m')] = \varepsilon_n \, \delta_{v,v'} \delta_{n,n'} \delta_{m,m'}. \qquad (15)$$

This treatment is valid in low energies as long as the magnetic field is not too strong, or $l_B \gg a$.

When the Fermi energy ε_F is inside a band gap of the spectrum, the Hall conductivity σ_{xy} is evaluated by the formula[43,44]

$$\sigma_{xy} = -e \left(\frac{\partial n_F}{\partial B} \right)_{\varepsilon_F}, \qquad (16)$$

where n_F is the electron density per unit area below the gap.

III. RESULTS AND DISCUSSION

We show the energy spectrum (left) and quantized Hall conductivity (middle) against the magnetic field amplitude for $\theta = 9.43^\circ$, 3.89° in Fig. 4, and for 2.65°, 1.47° in Fig. 5. In the rightmost panel, we show the zero-field band structure in the same energy range. The energy spectrum of $\theta = 9.43^\circ$ [Fig. 4(a)] is almost equivalent to the monolayer's Landau level, suggesting that two layers are nearly decoupled in this energy region. The sequence of the Hall conductivity, $4,12,20,\ldots$ in units of $-e^2/h$,[23,45,46] is exactly twice as large as the that of the monolayer.[1,2,40,41] Each Landau level is eightfold degenerate due to the number of layers as well as the spin and valley degeneracies.

In contrast, the energy spectrum of $\theta = 3.89^\circ$ [Figs. 4(d) and 4(e)] exhibits a complicated structure, which is clearly distinguished from monolayer graphene. In weak magnetic fields of $\Phi/\Phi_0 < 0.1$, the low-energy spectrum below 0.2 eV shows monolayerlike Landau levels and Hall conductivity of $4,12,20,\ldots$. In the higher-energy region above 0.2 eV, on the other hand, we observe holelike Landau levels moving downward in energy, and the negative Hall conductivity of $0,-4,-8,-12,\ldots$. When the electron density increases from the charge neutrality point, the Hall conductivity rises in a sequence of $4,12,20,\ldots$ with a step of 8, then abruptly drops to a negative extremum, and increases with a step of 4 all the way to zero.

Those spectral features in weak magnetic field perfectly coincide with the zero-field band structure in Fig. 4(f). The electronlike Landau levels are regarded as the quantized orbits accommodated in electron pockets at K and K' points, while the holelike Landau levels are those in a hole pocket at Γ point. The transition from electronlike levels to holelike levels corresponds to topological change of the Fermi surface at

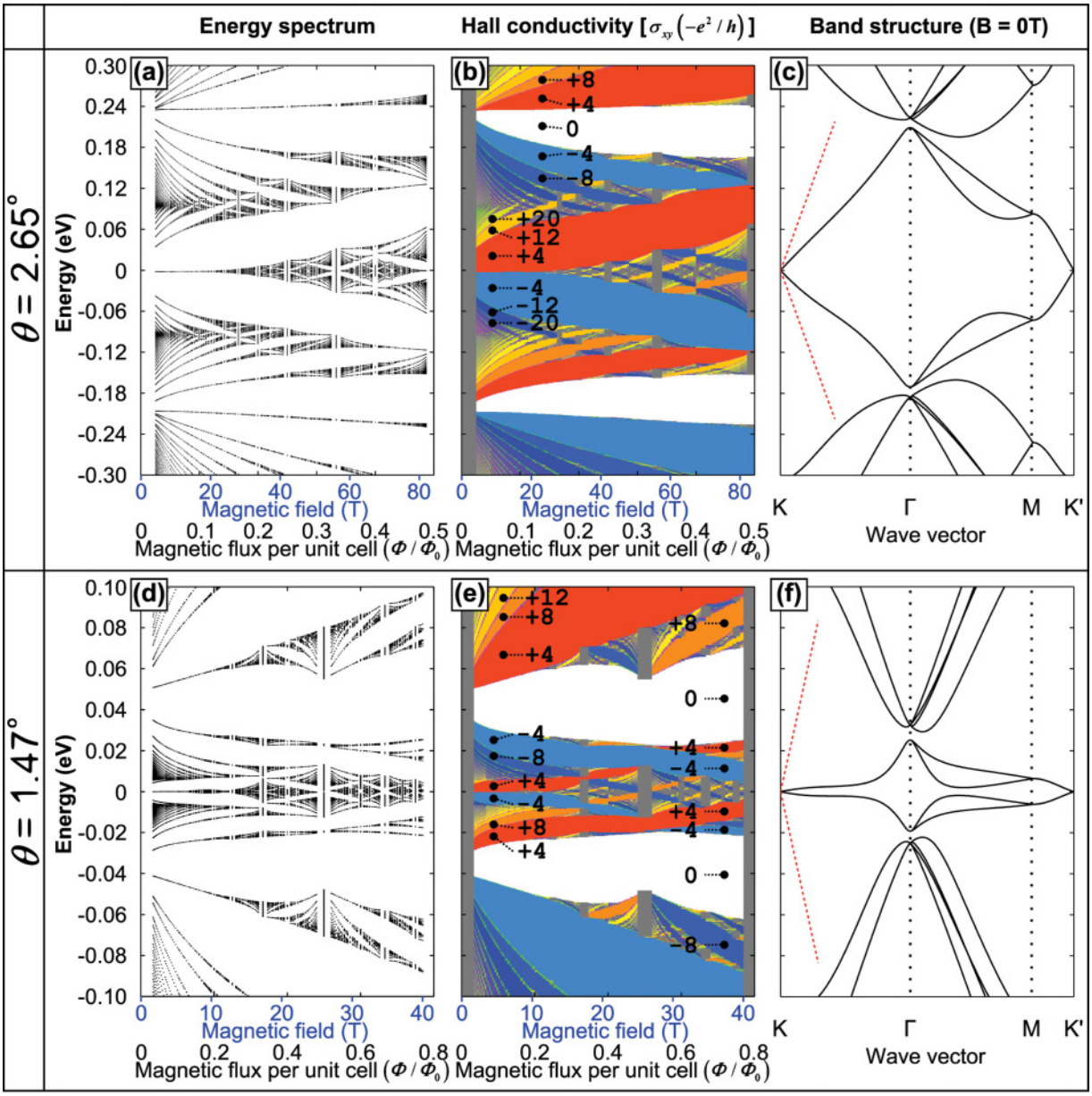

FIG. 5. (Color online) Plots similar to Fig. 4 for TBG with rotation angles of 2.65° (above) and 1.47° (below).

the saddle point (M point), which is responsible for the van Hove singularity at 0.2 eV. The step of the Hall conductivity reflects the number of electron and hole pockets in the first Brillouin zone, i.e., the degeneracy of an electronlike level is twice as large as that of a holelike level, because there are inequivalent K and K' points, whereas there is only one Γ point. Note that the pair of nearly degenerate lowest conduction bands [Fig. 3(f)] gives the identical Landau level energies and contributes to the degeneracy of two in addition to the spin degeneracy. Except for this doubling, the low-energy Landau level spectrum and the quantized Hall conductivity of TBG are quite analogous to those of whole π band in monolayer graphene,[47] as expected from the similarity of the band structure at zero magnetic field.

The electronlike and holelike Landau levels are alternatively explained by a nearly free electron model, without mentioning the rigorous zero-field band structure. In Fig. 6, we illustrate semiclassical electron trajectories at several different Fermi energies for a "free" TBG with interlayer coupling neglected. In the limit of a small Fermi energy [Fig. 6(a)], electrons move along closed orbits around K and K', and those motions are quantized into monolayerlike Landau levels. Since each of the K and K' points include two original K points from top and bottom monolayers, the Hall conductivity yields $4,12,20,\ldots$, i.e., double of monolayer's sequence. For large Fermi energies, the electron orbits around the K, and K' valleys cross each other as shown in Fig. 6(c). A finite interlayer coupling interchanges the orbits at each crossing point, and generates a single holelike trajectory moving around the Γ point in the opposite direction. The corresponding holelike Landau levels are fourfold degenerate due to spin and the Fermi circle doubling, and thus the Hall conductivity takes $0,-4,-8,-12,\ldots$. The middle panel [Fig. 6(b)] is for the intermediate energy region between two regimes. There, the different semiclassical orbits are strongly mixed by the magnetic breakdown due to a small k-space separation, resulting in broadening of Landau levels near the van Hove singularity in Fig. 4(d).

The electron density to fill the lowest conduction band is given by

$$n_0 = \frac{2g_s}{S}, \tag{17}$$

where g_s is the spin degeneracy and 2 is the band doubling. n_0 characterizes the order of the electron density required to reach the van Hove singularity and the holelike Landau levels. We have $n_0 = 3.5, 1.6$, and 0.5 in units of 10^{13} cm^{-2} for $\theta = 3.89^\circ$, 2.65°, and 1.47°, respectively. In monolayer graphene, the electron density to access the holelike levels is of the order of 10^{15} cm^{-2}.

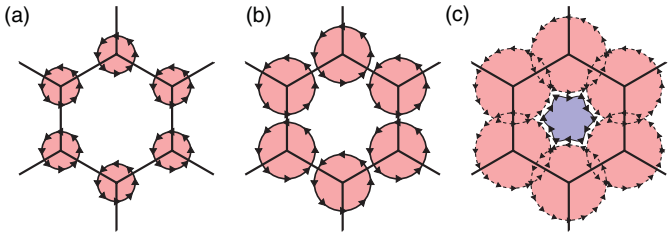

FIG. 6. (Color online) Fermi circle and electron trajectories of TBG in a nearly free electron picture, for three different Fermi energies (a) in the vicinity of Dirac points, (b) near van Hove singularity at the saddle point, and (c) holelike band at the Γ point.

The semiclassical picture breaks down when the magnetic field is so strong that

$$l_B \lesssim L \tag{18}$$

because then the uncertainty in electron momentum ($\sim 2\pi/l_B$) becomes comparable or larger than the size of the Brillouin zone ($\sim 2\pi/L$), and a semiclassical cyclotron orbit is not well defined anymore. Then, the energy spectrum, including even $n = 0$ Landau level, exhibits a fractal band structure.[20,21] The magnetic field strength needed to observe a fractal structure becomes more feasible in smaller rotation angles due to larger unit-cell size L. The condition $l_B \lesssim L$ is equivalent to $\Phi/\Phi_0 \gtrsim \sqrt{3}/(4\pi) \approx 0.14$, which amounts to $B \gtrsim 50$, 23, and 7.2 T for $\theta = 3.89^\circ$, 2.65°, and 1.47°, respectively. In Fig. 4, we actually observe that the electron and hole Landau levels gradually evolve into the fractal structure as the magnetic field exceeds the critical value. The Hall conductivity in the fractal regime behaves nonmonotonically as a function of Fermi energy.[25,26]

The energy spectrum of $\theta = 3.89^\circ$ and that of $\theta = 2.65^\circ$ (Fig. 5) exhibit similar structures except for the energy scale, as expected from the resemblance between the band structures argued in the previous section. In the case of $\theta = 1.47^\circ$, the spectrum is strongly compressed in the vicinity of Dirac points, in accordance with the bandwidth reduction in small rotation angles. Although the band structure near Dirac points is almost flat, the Γ point still has a finite band velocity which is about $0.6v$. As a consequence, the energy gaps between the holelike Landau levels are much wider than those between the electronlike levels.

While we have considered some specific commensurate angles, a similar fractal energy spectrum should appear in any small angles including incommensurate ones, as long as the lattice structure exhibits a long-period Moiré pattern. As a natural extension of the previous argument, the condition for the fractal spectrum in general angles is expected to be

$$l_B \lesssim L_{\mathrm{M}} \tag{19}$$

instead of Eq. (18), where L_{M} is the period of the Moiré pattern given by[28,48]

$$L_{\mathrm{M}} = \frac{a}{2\sin(\theta/2)}. \tag{20}$$

Note that L_{M} is a continuous function of θ, while the rigorous unit-cell size L discontinuously changes depending on the commensurability of lattice periods and diverges in incommensurate angles. L_{M} coincides with L only in commensurate angles with $|m-n| = 1$, which are the cases considered in this paper. The condition of Eq. (19) is rewritten as

$$B \gtrsim \frac{4\hbar}{ea^2}\sin^2\frac{\theta}{2} \approx 3.3\ (\mathrm{T}) \times [\theta\ (\mathrm{degree})]^2, \tag{21}$$

which quantifies the magnetic field required for the fractal spectrum as a function of the rotation angle.

IV. CONCLUSION

We investigated the electronic structure and the quantum Hall effect in TBG with various rotation angles in the presence of magnetic field. We calculated the energy spectrum and quantized Hall conductivity in a wide magnetic field range, and described the evolution from the semiclassical Landau levels to the fractal band structure. In weak magnetic field, the low-energy conduction band is quantized into electronlike and holelike Landau levels in accordance with the structure of the folded energy band. In increasing magnetic field, those semiclassical levels gradually evolve into Hofstadter's butterfly, where the Hall conductivity exhibits a nonmonotonic behavior as a function of Fermi energy. The typical electron density and magnetic field amplitude characterizing the spectrum monotonically decrease as the rotation angle is reduced, indicating that the rich electronic properties may be observed in a moderate condition for TBG with small angle less than 5°.

ACKNOWLEDGMENTS

This work was supported by JST-EPSRC Japan-UK Cooperative Programme Grant No. EP/H025804/1. P.M. acknowledges the support from Grant-in-Aid for Research Activity Start-up (23840004) by Japan Society for the Promotion of Science (JSPS), and appreciates the support from Korea Institute of Science and Technology Information Supercomputing Center through the strategic support program for the supercomputing application research (Grant No. KSC-2009-S02-0009), and the Supercomputer Center, Institute for Solid State Physics, University of Tokyo for the use of the facilities (Project No. ID: H23-D-0009).

[1] K. S. Novoselov, A. K. Geim, S. V. Morozov, D. Jiang, M. I. Katsnelson, I. V. Grigorieva, S. V. Dubonos, and A. A. Firsov, Nature (London) **438**, 197 (2005).
[2] Y. Zhang, Y.-W. Tan, H. L. Stormer, and P. Kim, Nature (London) **438**, 201 (2005).
[3] K. S. Novoselov, E. McCann, S. V. Morozov, V. I. Fal'ko, M. I. Katsnelson, U. Zeitler, D. Jiang, F. Schedin, and A. K. Geim, Nat. Phys. **2**, 177 (2006).
[4] E. McCann and V. I. Falko, Phys. Rev. Lett. **96**, 086805 (2006).
[5] C. Berger, Z. Song, X. Li, X. Wu, N. Brown, C. Naud, D. Mayou, T. Li, J. Hass, A. N. Marchenkov, E. H. Conrad, P. N. First, and W. A. de Heer, Science **312**, 1191 (2006).
[6] J. Hass, R. Feng, J. E. Millan-Otoya, X. Li, M. Sprinkle, P. N. First, W. A. de Heer, E. H. Conrad, and C. Berger, Phys. Rev. B **75**, 214109 (2007).
[7] J. Hass, F. Varchon, J. E. Millán-Otoya, M. Sprinkle, N. Sharma, W. A. de Heer, C. Berger, P. N. First, L. Magaud, and E. H. Conrad, Phys. Rev. Lett. **100**, 125504 (2008).
[8] A. Luican, G. Li, A. Reina, J. Kong, R. R. Nair, K. S. Novoselov, A. K. Geim, and E. Y. Andrei, Phys. Rev. Lett. **106**, 126802 (2011).
[9] R. Zhao, Y. Zhang, T. Gao, Y. Gao, N. Liu, L. Fu, and Z. Liu, Nano Res. **4**, 712 (2011).
[10] G. Li, A. Luican, J. M. B. Lopes dos Santos, A. H. Castro Neto, A. Reina, J. Kong, and E. Y. Andrei, Nat. Phys. **6**, 109 (2009).
[11] J. Hass, W. A. d. Heer, and E. H. Conrad, J. Phys.: Condens. Matter **20**, 323202 (2008).
[12] D. L. Miller, K. D. Kubista, G. M. Rutter, M. Ruan, W. A. de Heer, P. N. First, and J. A. Stroscio, Phys. Rev. B **81**, 125427 (2010).
[13] D. L. Miller, K. D. Kubista, G. M. Rutter, M. Ruan, W. A. de Heer, M. Kindermann, P. N. First, and J. A. Stroscio, Nat. Phys. **6**, 811 (2010).
[14] Z. Ni, Y. Wang, T. Yu, Y. You, and Z. Shen, Phys. Rev. B **77**, 235403 (2008).
[15] L. Xie, H. Wang, C. Jin, X. Wang, L. Jiao, K. Suenaga, and H. Dai, J. Am. Chem. Soc. **133**, 10394 (2011).
[16] S. Latil, V. Meunier, and L. Henrard, Phys. Rev. B **76**, 201402 (2007).
[17] J. M. B. Lopes dos Santos, N. M. R. Peres, and A. H. Castro Neto, Phys. Rev. Lett. **99**, 256802 (2007).
[18] S. Shallcross, S. Sharma, and O. A. Pankratov, Phys. Rev. Lett. **101**, 056803 (2008).
[19] E. Suárez Morell, J. D. Correa, P. Vargas, M. Pacheco, and Z. Barticevic, Phys. Rev. B **82**, 121407(R) (2010).
[20] D. R. Hofstadter, Phys. Rev. B **14**, 2239 (1976).
[21] R. Bistritzer and A. H. MacDonald, Phys. Rev. B **84**, 035440 (2011).
[22] J. D. Sanchez-Yamagishi, T. Taychatanapat, K. Watanabe, T. Taniguchi, A. Yacoby, and P. Jarillo-Herrero, Phys. Rev. Lett. **108**, 076601 (2012).
[23] D. S. Lee, C. Riedl, T. Beringer, A. H. Castro Neto, K. von Klitzing, U. Starke, and J. H. Smet, Phys. Rev. Lett. **107**, 216602 (2011).
[24] I. Crassee, J. Levallois, D. van der Marel, A. L. Walter, Th. Seyller, and A. B. Kuzmenko, Phys. Rev. B **84**, 035103 (2011).
[25] M. Kohmoto, Ann. Phys. (NY) **160**, 355 (1985).
[26] D. J. Thouless, M. Kohmoto, M. P. Nightingale, and M. den Nijs, Phys. Rev. Lett. **49**, 405 (1982).
[27] E. J. Mele, Phys. Rev. B **81**, 161405(R) (2010).
[28] S. Shallcross, S. Sharma, E. Kandelaki, and O. A. Pankratov, Phys. Rev. B **81**, 165105 (2010).
[29] T. Nakanishi and T. Ando, J. Phys. Soc. Jpn. **70**, 1647 (2001).
[30] S. Uryu, Phys. Rev. B **69**, 075402 (2004).
[31] J. C. Slater and G. F. Koster, Phys. Rev. **94**, 1498 (1954).
[32] G. Trambly de Laissardiére, D. Mayou, and L. Magaud, Nano Lett. **10**, 804 (2010).
[33] Y. Wang, Z. Ni, L. Liu, Y. Liu, C. Cong, T. Yu, X. Wang, D. Shen, and Z. Shen, ACS Nano **4**, 4074 (2010).
[34] Z. Ni, L. Liu, Y. Wang, Z. Zheng, L.-J. Li, T. Yu, and Z. Shen, Phys. Rev. B **80**, 125404 (2009).
[35] R. Bistritzer and A. H. MacDonald, Proc. Natl. Acad. Sci. USA **108**, 12233 (2011).
[36] E. Brown, Solid State Phys. **22**, 313 (1968).
[37] D. Xiao, M.-C. Chang, and Q. Niu, Rev. Mod. Phys. **82**, 1959 (2010).
[38] J. W. McClure, Phys. Rev. **104**, 666 (1956).
[39] N. H. Shon and T. Ando, J. Phys. Soc. Jpn. **67**, 2421 (1998).

[40]Y. Zheng and T. Ando, Phys. Rev. B **65**, 245420 (2002).
[41]V. P. Gusynin and S. G. Sharapov, Phys. Rev. Lett. **95**, 146801 (2005).
[42]T. Ando, J. Phys. Soc. Jpn. **74**, 777 (2005).
[43]P. Streda, J. Phys. C: Solid State Phys. **15**, L717 (1982).
[44]A. Widom, Phys. Lett. A **90**, 474 (1982).
[45]R. de Gail, M. O. Goerbig, F. Guinea, G. Montambaux, and A. H. Castro Neto, Phys. Rev. B **84**, 045436 (2011).
[46]M.-Y. Choi, Y.-H. Hyun, and Y. Kim, Phys. Rev. B **84**, 195437 (2011).
[47]Y. Hatsugai, T. Fukui, and H. Aoki, Phys. Rev. B **74**, 205414 (2006).
[48]T. A. Green and J. Weigle, Helv. Phys. Acta **21**, 217 (1948).